

Breakup of liquid jets from non-circular orifices

Priyesh Sharma · Tiegang Fang

Received: 27 August 2013/Revised: 3 January 2014/Accepted: 6 January 2014/Published online: 21 January 2014
© Springer-Verlag Berlin Heidelberg 2014

Abstract The purpose of this investigation is to study the effect of the orifice geometry on liquid breakup. In order to develop a better understanding of the liquid jet breakup, investigations were carried out in two steps—study of low-pressure liquid jet breakup and high-pressure fuel atomization. This paper presents the experimental investigations conducted to study the flow behavior of low-pressure water jets emanating from orifices with non-circular geometries, including rectangular, square, and triangular shapes and draws a comparison with the flow behavior of circular jets. The orifices had approximately same cross-sectional areas and were machined by electro-discharge machining process in stainless steel discs. The liquid jets were discharged in the vertical direction in atmospheric air at room temperature and pressure conditions. The analysis was carried out for gage pressures varying from 0 to 1,000 psi (absolute pressures from 0.10 to 6.99 MPa). The flow behavior was analyzed using high-speed visualization techniques. To draw a comparison between flow behavior from circular and non-circular orifices, jet breakup length and width were measured. The flow characteristics were analyzed from different directions, including looking at the flow from the straight edges of the orifices as well as their sharp corners. The non-circular geometric jets demonstrated enhanced instability as compared to the circular jets. This has been attributed to the axis-switching phenomenon exhibited by them. As a result, the non-circular jets yielded shorter breakup lengths as compared to the circular jets. In order to

demonstrate the presence of axis-switching phenomenon in square and triangular jets, the jet widths were plotted along the axial direction. This technique clearly demonstrated the axis switching occurring in square and triangular jets, which was not clearly visible unlike the case of rectangular jets. To conclude, non-circular geometry induces greater instabilities in the liquid jets, thereby leading to faster disintegration. Thus, non-circular orifice geometries can provide a cheaper solution of improving liquid breakup and thus may enhance fuel atomization as compared to the precise manufacturing techniques of drilling smaller orifices or using costly elevated fuel injection pressure systems.

1 Introduction

Fuel atomization plays an important role as reduction in fuel drop size increases mixing rates; lowers exhaust emissions; and determines the combustion efficiency, power output, and fuel economy of an internal combustion engine (Lefebvre 1985; Reeves and Lefebvre 1986; Rink and Lefebvre 1986). Primarily, most engines use high-pressure fuel injection with small orifices for achieving better atomization (Woodyard 2004; Rayleigh 1879). Higher pressures impose limitations on the safe working loads of the fuel injection system and precise manufacturing, thereby increasing the equipment cost. Further, smaller orifices are difficult to manufacture and are prone to blockage. This calls for looking at the basics of the atomization process. Atomization is one of the different modes of the liquid jet breakup. The breakup of a liquid jet emanating from an orifice is a ubiquitous phenomenon of nature with wide applications (Lefebvre 1989; Zelenka et al. 1990).

P. Sharma · T. Fang (✉)
Department of Mechanical and Aerospace Engineering, North Carolina State University, 911 Oval Drive-Campus Box 7910, Raleigh, NC 27695, USA
e-mail: tfang2@ncsu.edu

Liquid jet breakup is influenced by the design of the nozzle, the jet's velocity and turbulence, and the physical and thermal properties of both liquid and surrounding gas (Bidone 1829; Savart 1833; Plateau 1873). The breakup length of the jet, which is defined as the length of the jet from the nozzle tip to first drop breakup, defines the breakup regimes. So far, the research on liquid jet breakup has concentrated majorly on circular orifices though there has been interest in studying the effect of asymmetric orifices since the nineteenth century. Rayleigh (1878) analyzed the experimental works of Bidone (1829) and reported the axis-switching phenomenon observed in jets issued from non-circular orifices. Results of the investigations on jets issued from non-circular orifices show that non-circular geometry of the orifice tends to provide an efficient technique of passive flow control at a relatively cheaper cost as it involves changes in the geometry of the nozzle only.

The purpose of this investigation is to study the effect of the orifice geometry on liquid breakup. Efforts are put into determine if better spray atomization, smaller droplet size, and better air–fuel mixing can be achieved by inducing enhanced instabilities in the spray by non-circular geometry of the orifice. In order to develop a better understanding of the liquid jet breakup, investigations were carried out in two steps—study of low-pressure liquid jet breakup and high-pressure fuel atomization (which was reported in a separate publication). Although a lot of work has been carried out previously on non-circular orifices like ellipse, it is very difficult to find such works that have extensively studied other non-circular shapes like square and triangles and even rectangle and ellipse for liquid jet pressures varying up to 1,000 psi (absolute 6.99 MPa). This paper focuses on the flow behavior observed at injection pressures as high as 1,000 psi. The results can provide some insights as a bridge to understand fuel atomization under much higher pressure (around 15,000 psi or 100 MPa).

2 Literature review

2.1 Disintegration of liquid jets from a circular orifice

The early investigations of the breakup of a liquid jet emanating into another fluid dates back more than a century (Bidone 1829; Savart 1833; Plateau 1873; Rayleigh 1878). By neglecting the effects of ambient gas density, jet liquid viscosity, and the gravitational forces, Rayleigh (1878) demonstrated that a cylindrical laminar jet issued in still air is unstable with respect to the disturbances of wavelengths larger than the jet circumference and calculated the initial drop size. These predictions were later confirmed experimentally by Tyler (1933). Weber (1931)

extended the works of Rayleigh to viscous liquids and included the effects of ambient gas density, but his theoretical predictions did not agree well with the experimental data as pointed out by Sterling and Sleicher (1975).

The disintegration of a liquid jet can now be classified into distinct regimes of breakup. The regimes are due to the action of dominant forces on the jet, leading to its breakup, and it is important that these forces be identified in order to explain the breakup mechanism in each regime (Reitz and Bracco 1986). A cylindrical liquid jet emanated in stagnant gas undergoes four different breakup regimes depending on the interaction of the liquid inertia, surface tension, and aerodynamic forces acting on the jet. The different jet breakup regimes can be schematically shown on a plot of varying breakup length of the jet as a function of jet velocity, keeping all other parameters constant as reviewed by Grant and Middleman (1966). The four different breakup regimes include Rayleigh breakup regime, first wind-induced regime, second wind-induced regime, and atomization regime (Reitz and Bracco 1982; Lin and Reitz 1998; Lin 2003). Mathematical analysis of these regimes was discussed by Lin (1996).

The criteria for demarcating the different regimes of a cylindrical liquid jet emanated in still air have been numerically quantified. Ranz (1956) determined that Rayleigh breakup occurs and the formation of jet occurs if jet liquid Weber number, $We_L > 8$, where $We_L = \frac{\rho_L U^2 D}{\sigma}$. The criterion ambient gas Weber number $We_G \equiv \frac{\rho_G U^2 D}{\sigma} < 0.4$ corresponds to the point where the inertia force of the surrounding gas reaches about 10 % of the surface tension forces. ρ_L and ρ_G are the liquid and gas densities, U is the jet initial velocity, and D is the orifice diameter. Numerical results of Sterling and Sleicher (1975) indicate that the onset of first wind-induced regime occurs when $We_L = 1.2 + 3.41 Z_L^{0.9}$, where $Z_L \equiv \frac{We_L^{0.5}}{Re_L}$, $Re_L \equiv U(D_h)/\nu_L$. Hence, the criteria for Rayleigh breakup would be

$$We_L > 8 \text{ and } We_G < 0.4 \text{ or } We_G < 1.2 + 3.41 Z_L^{0.9}. \quad (1)$$

Ranz (1956) further argued that the gas inertia is of the same order as the surface tension force when $We_G = 13$. This marks the end of the first wind-induced regime. Thus, the limits for the first induced regime are

$$1.2 + 3.41 Z_L^{0.9} < We_G < 13. \quad (2)$$

Moreover, $We_G = 13$ also indicates the beginning of the second wind-induced regime where the aerodynamic forces start to become dominant. Miesse (1955) suggested the criterion for the onset of atomization as $We_G > 40.3$. Hence, the limits for the second wind-induced regime can be defined as

$$13 < We_G < 40.3. \quad (3)$$

However, it should be noted that these breakup criteria based on We_G did not consider the internal flow effects and the nozzle geometry such as the length-to-diameter ratio (Lin and Reitz 1998). Therefore, these criteria can only provide rough regimes for jet breakup.

2.2 Disintegration of liquid jets from non-circular orifices

Till date, majority of the research work has been carried out on the jets issued from circular orifices. Few studies have considered the asymmetrical orifice geometries. However, the interest in non-circular orifices dates back to the days of Bidone (1829). Rayleigh (1878) analyzed Bidone's observations and reported about the unique phenomenon of axis switching demonstrated by the jets from non-circular orifices. Citing the experiment of Bidone, Rayleigh (1945) stated, "Thus in the case of an elliptical aperture, with major axis horizontal, the sections of the jet taken at increasing distances gradually lose their ellipticity until at a certain distance the section is circular. Further out the section again assumes ellipticity, but now with the major axis vertical." The surface tension force of the liquid is considered responsible for this unique phenomenon. The geometrical transformation superimposed with the axial motion of jet gives rise to the axis-switching profile on the jet (Kasyap et al. 2009). This geometrical oscillation from elliptical to circular and back to elliptical cross section persists until damped by the viscous forces or the jet breaks up downstream owing to the growth of instabilities on its surface. Kasyap et al. (2008, 2009) experimentally studied the axis-switching and breakup length of elliptic liquid jets and showed that the elliptic jets exhibit more unstable behavior and, hence, have a shorter breakup length than a corresponding circular liquid jet. Furthermore, they discussed the effect of ellipticity on breakup length and showed that increasing the ellipticity in some ranges makes the elliptic liquid jet more unstable.

These results clearly indicate that asymmetric geometry of nozzle orifices provides a very effective passive control over jet breakup phenomenon and introduces enhanced instabilities, thereby reducing breakup length and droplet size and, in some cases, improving mass entrainment with better mixing. As can be seen, among all the non-circular orifice geometries, elliptical orifices have been studied extensively. The elliptical jets present an intermediate case between round and planar jets. The main advantage of elliptical cross section over circular case is that it facilitates rapid mixing and spreading when the liquid is discharged into another fluid (Gutmark and Grinstein 1999). The azimuthal curvature variation in an elliptic jet makes the flow feature very complex. Even in diesel spray applications, under some experimental conditions, elliptical nozzles

have shown better performance than circular nozzles. The elliptic spray angle is much larger than that of the circular spray, while the Sauter mean diameter (SMD) of elliptic sprays is much smaller than that of circular sprays (Yunyi et al. 1998). Furthermore, Messina and Acharya (2006) studied experimentally the velocity field and spreading rate of a liquid spray issued from an elliptic nozzle with and without primary air. By actively controlling the air flow, they manipulated the mixing and dispersion of the spray. In comparison with a circular nozzle, the spray issued from an elliptic nozzle provides better mixing in terms of higher mass entrainment and greater jet width.

The rectangular orifice presents a special case. It incorporates the features of aspect ratio, similar to an elliptical orifice, and the effects of corners, similar to square and triangular orifices. Herzberg and Ho (1995) found that the crossover location is directly proportional to the aspect ratio of the orifice. Similar to the Rayleigh's analysis (Rayleigh 1879) for a cylindrical jet, Drazin and Reid (1981) conducted stability analysis for planar jets. They found that an inviscid infinite plane jet is stable to all the disturbances because surface tension always has a damping effect and forces the surface back to its initial shape when perturbed as the minimum energy occurs when the two surfaces are parallel. However, a finite planar jet is always unstable to the surface tension instabilities in the form of surface ripples as the initial shape is not stable to any changes that bring the jet closer to the cylindrical shape. Thus, the basic tendency is toward contraction, which occurs with considerable inertial overshoot, leading to axis-switching phenomenon. Moreover, according to Soderberg and Alfredson (1998), the jet is also subjected to the process of velocity profile relaxation as it is issued from the nozzle. The interaction of the relaxation of the boundary layer or turbulent eddies with the free surface tension and acceleration due to gravity generates potentially unstable waves that grow in amplitude downstream and contribute to the jet breakup. Konkachbaev et al. (2000) observed axis-switching phenomena in slab jets and explained it a result of surface tension and corner vortices.

Based upon these reviews, it can be concluded that the non-circular orifices can induce enhanced instabilities in the jets. Many of the research works done on the elliptical orifices have clearly shown that they undergo axis-switching phenomenon, which quickens the disintegration process of the jet. Thus, the non-circular jets are more unstable. Despite such major changes and advantages over circular orifices, there are few works that have extensively studied other non-circular shapes like square and triangles and even rectangle and ellipse for liquid jet pressures varying up to 1,000 psi (absolute 6.99 MPa). Note that the pressure in the bracket after the gage pressure in psi is the absolute pressure in MPa. For brevity, the word "absolute"

is omitted in the following. The objective of this work is to explore the scope of investigation in the areas of non-circular liquid jets. The results obtained have been compared to those obtained from the circular orifices. Based upon our findings, we have tried to improve our understanding of the basic physical processes involved in jet breakup and atomization.

3 Experimental setup and procedure

The liquid injection system consisted of a stainless steel water storage tank pressurized to supply high-pressure water to the orifice. The tank pressure was controlled using regulated compressed nitrogen. A filter was installed to filter out any contaminants. The liquid flow to the orifice was controlled using a flow control valve along with a digital pressure gauge to monitor the injection pressure and pressure drops occurring in the supply system. An orifice assembly (Fig. 1a) was designed and comprised of a cylindrical smoothing chamber of 5 mm diameter and about 32 mm long, which delivered water to the orifice plate. The orifice plate was installed in the orifice assembly. The orifice plates were fabricated using stainless steel, and the circular and non-circular orifices were machined using electro-discharge machining (EDM) process. The geometrical details of the orifices are provided in Table 1. Figure 1b shows the high-resolution image of the different orifices used in the present study. Water was used as the working liquid, and properties are listed in Table 2. The gage injection pressure was varied from 0 to 1,000 psi (from 0.10 to 6.99 MPa). Gage pressure 0 psi (0.10 MPa) corresponds to no external pressure, and the liquid was allowed to fall freely under the hydrostatic pressure of the water column due to gravity. The jets were discharged into quiescent ambient air. Care was taken to ensure that the non-circular orifices had a cross-sectional area approximately equal to the corresponding circular orifice. A front lighting system was used to illuminate the jet. A high-speed camera (Phantom 4.3) with a Nikon[®] 50-mm f/1.8 lens was used to capture the jet images. The pixel resolution was varied as per the requirement in order to capture the details of the breakup and axis-switching phenomena. Majority of images were captured at a frame rate of 14,035 frames per second with a pixel resolution of 32 × 600. For jets requiring a closer shot, pixel resolution was increased to 64 × 600 at a frame rate of 10,256 fps. In order to observe the geometrical development of the jets from the non-circular orifices, the jets were analyzed from different orientations or view planes, including those containing the straight edges and those containing the sharp corners or vertices. Both the nitrogen gas supply pressure and the water injection pressure were noted. No appreciable

differences in the two pressures were observed; hence, negligible pressure drop occurred in the supply system. This also means that the hydrostatic pressure of the water column was also negligible and, hence, has not been included in the measurements.

The experiments were conducted for a wide range of flow conditions. The different flow parameters have been calculated using the hydraulic diameters of each orifice and the steady-state mass flow rate measurements. The steady-state mass flow rates were measured using a precise spring balance and stopwatch. The discharged liquid was allowed to attain its steady state and then collected in a vessel. Based upon the pre-injection and post-injection masses of the vessel and the time duration recorded in the stopwatch, mass flow rates were calculated using the following relation

$$\dot{m} = \frac{m_f - m_i}{\Delta t} \quad (4)$$

where m_f is the post-injection mass of the collecting vessel, m_i is the pre-injection mass of the collecting vessel, and Δt is the time recorded on the stopwatch.

Mass flow rate was measured five times for each injection pressure and an average was then calculated. Using the mass flow rate values, volumetric flow rates and then jet exit velocities were calculated. Based on the exit velocities obtained, coefficients of discharge (CD) were calculated for each injection pressure and all values obtained were <1. For each injection pressure, five measurements were taken for the high-speed imaging. In each measurement, 1,000 images were saved for post-processing. The high-speed jet images were then processed and calculations were carried out on them, and parameters, like breakup length and jet width, were calculated for each of the 1,000 images. Final values have been obtained by taking an average of the 1,000 measurements and then averaged over the five measurements.

4 Results and discussion

As discussed earlier, jet breakup depends on the fluid flow conditions, which can be well represented in the form of non-dimensional numbers (Ohnesorge 1936; Reitz 1978). The breakup process is defined for the parameter $\sqrt{We_L}$ as it provides the linear dependence of the process on jet velocity.

4.1 Comparison of flow behavior from different orifices

4.1.1 Steady-state mass flow rate measurements

The steady-state mass flow rates from different orifices for injection pressures varying from 0 to 1,000 psi (from 0.10

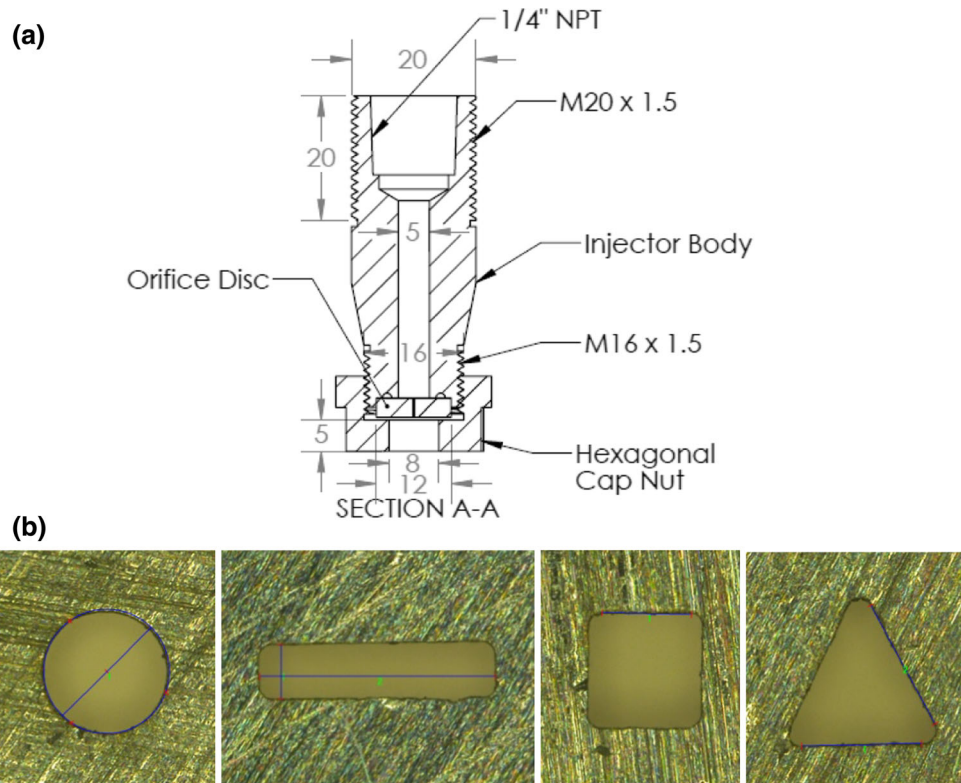


Fig. 1 Experimental setup of nozzles: **a** drawing of nozzle assembly; **b** different orifices used in the experiments (from left to right): *circular* orifice—dia: 308 μm; *rectangular* orifice—

571 μm × 129 μm; *square* orifice—side: 276 μm × 276 μm; *triangular* orifice—side: 288 μm × 325 μm × 338 μm (not include the corner arc sections)

Table 1 Geometrical details of the orifices (units in mm)

	Area (mm ²)	% Diff. in area	D _h (mm)	L/D _h ratio
Circle	7.4285 × 10 ⁻²	–	0.3075	4.13
Rectangle	7.3829 × 10 ⁻²	-0.617	0.2110	6.01
Square	7.5911 × 10 ⁻²	2.188	0.2879	4.41
Triangle	7.2188 × 10 ⁻²	-2.82	0.2559	4.96

Table 2 Physical properties of water

Properties at 20 °C	
Density of water (kg/m ³)	998.2
Viscosity (Pa s)	0.001
Surface tension (N/m)	0.0729
Density of air (kg/m ³)	1.204

to 6.99 MPa) are presented in Fig. 2a. As it can be seen, the mass flow rates are nearly the same for lower injection pressures; however, for gage pressures above 200 psi (1.48 MPa), rectangular orifice with slightly higher area discharges higher mass flow rate as compared to the other cases. Based upon the mass flow rate measurements obtained as shown above, the volumetric flow rate, Q, was

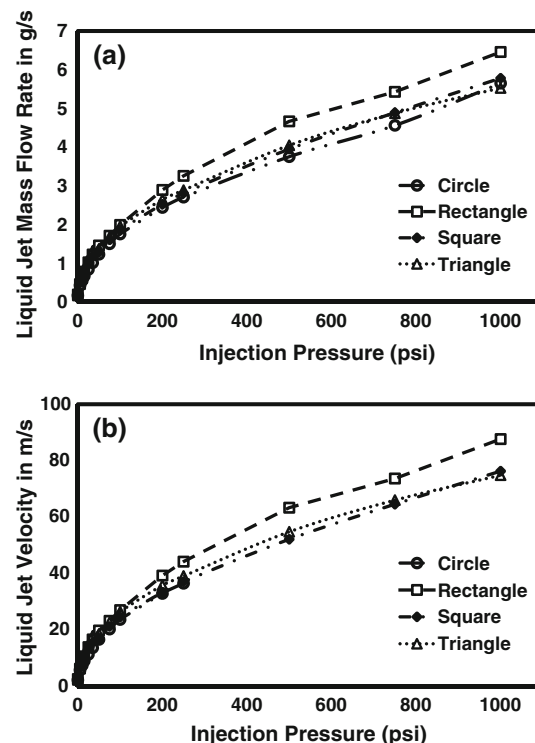


Fig. 2 The steady-state mass flow rate (a) and exit velocity (b) for different orifices under different pressures

calculated and, thus, the jet exit velocity was obtained using the relation

$$V_e = Q/A_e \quad (5)$$

where A_e is the area of the orifice and V_e is the jet exit velocity. As the rectangular orifice has slightly higher flow rate, as a result, the jet exit velocity is slightly higher than the other cases as shown in Fig. 2b. The same jet exit velocity is used for calculating the non-dimensional numbers for characterizing the flow conditions at different injection pressures. The coefficient of discharge for each injection pressure was also calculated using the relation

$$C_D = \frac{V_e}{V_{ideal}} \quad (6)$$

The ideal jet exit velocity at each injection pressure was calculated using the following relation

$$V_{ideal} = \sqrt{\frac{2\Delta P}{\rho_f}} \quad (7)$$

where ΔP is the pressure differential between the gauge location and the orifice exit (i.e., the ambient).

4.1.2 Reynolds number and Weber number

Reynolds number is a dimensionless parameter that gives the ratio of the inertial forces of the jet flow to the viscous forces of the fluid. It can be calculated using the following relation:

$$Re = \frac{\rho_f V_e D_h}{\mu} \quad (8)$$

where ρ_f is the jet fluid density, V_e is the jet exit velocity, D_h is the hydraulic diameter of the orifice, and μ is the dynamic viscosity of the fluid. The hydraulic diameter of non-circular orifices can be calculated using the following relation:

$$D_h = \frac{4 \times A_e}{P} \quad (9)$$

where P is the perimeter of the non-circular geometry. The variation of the Reynolds number for the flow from different orifices at varying pressure conditions is presented in Fig. 3. Two critical Reynolds numbers (2,100 and 4,000) are marked in the figures to show the transition regime (Munson et al. 2013). It can be noted that the flow behavior is close for the circular-, square-, and triangular-shaped orifices at lower injection pressures. However, at higher pressures, the level of turbulence is highest in the circular orifice followed by the square and then the triangle. Turbulence is the lowest in the flow from rectangular orifice. In fact, it is interesting to note that in case of rectangular

orifice, the flow remains laminar even at 15 psi (0.20 MPa) while for the other cases, it has already entered the transition zone at 10 psi (0.17 MPa) assuming a critical Reynolds number of 2,100. Moreover, flow from the square orifice is the first to show turbulence as can be seen in the figure.

The most important parameter in characterizing the jet breakup is the Weber number as it gives the ratio between the fluid inertia and the surface tension forces. It can be obtained using the following relation:

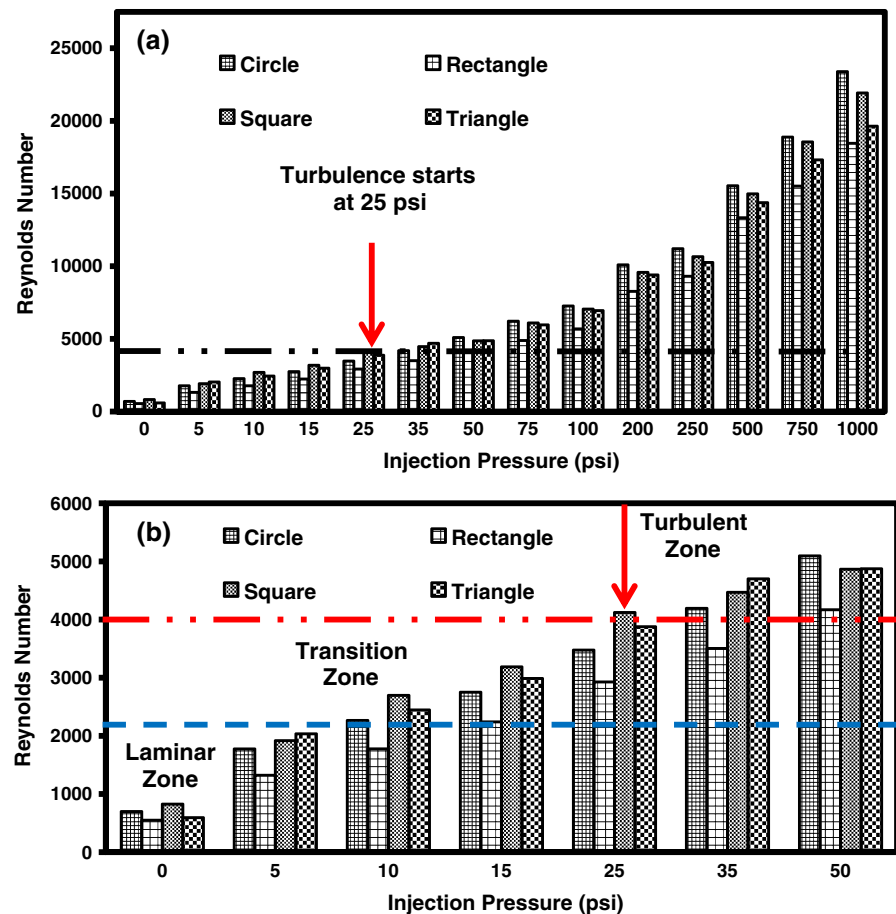
$$We_L = \frac{\rho_f V_e^2 D_h}{\sigma}, \quad We_G = \frac{\rho_g V_e^2 D_h}{\sigma} \quad (10a \text{ and } 10b)$$

where ρ_f is the density of the jet liquid, ρ_g is the density of the ambient gas, V_e is the jet fluid exit velocity, D_h is the hydraulic diameter of the orifice shape, σ is the fluid surface tension. With the variation in jet exit velocity, the Weber number for the jet liquid as well as the ambient gas changes. As mentioned earlier, the Weber number gives the criteria for the different jet breakup regimes. For liquid breakup, although viscosity plays an important role in this process, its effects mainly exist in the internal flow inside the nozzle. As long as the liquid comes out of the nozzle, the breakup is mainly determined by surface tension and aerodynamic force due to the motion of the fluid. The Weber number is a proper parameter showing the effects of these two forces. The variation in We_L and We_G is shown in Figs. 4 and 5, respectively, for the different orifices. The Weber number for both the jet liquid as well as the ambient gas has increased relatively linearly with the injection pressure. The Weber number for each orifice is different even though the injection pressures are same. However, the values are in a close range. Important to note is that, even at pressure as high as 1,000 psi (6.99 MPa), the gas Weber number, We_G , of the jets from any of the orifices has not crossed the value of 40.3, which is the mark of onset of the atomization regime (Miesse 1955). Thus, the jets obtained from all the cases have undergone breakup up to second wind-induced breakup regime only.

4.2 Development of jet with the injection pressure

Image sequences are used to present the breakup behavior of liquid jets for different injection pressures or $\sqrt{We_L}$ conditions. The viewing area is confined to the immediate vicinity of the breakup location. Since the breakup length is different for each orifice, in order to capture the jet breakup phenomenon, it was required to set up the high-speed camera at different locations with different resolutions. Thus, the images displayed are not up to the same scale. However, while measuring, the length proper scale factor was used corresponding to the resolution used. As has already been mentioned, for different orifices, the Weber

Fig. 3 The Reynolds number under different pressures for the four orifices: **a** entire pressure range; **b** magnified view in the lower range of injection pressures



numbers and, thus, the flow conditions differ even if the injection pressure is same.

4.2.1 Circular orifice

The circular jets under different pressures are shown in Fig. 6. The breakup length for the circular orifice was found out to be very long as compared to the other cases. Owing to the limitation of the high-speed camera's field of view, it was not possible at some pressures to capture the entire breakup process of the circular orifice in one shot. Hence, the photographs of the jet were taken at different axial locations and at different instants. However, they have been patched up together with no spatial discontinuity. The breakup of the circular liquid jet is axisymmetric at low $\sqrt{We_L}$ in nature as predicted by Rayleigh (1945). As per the calculations, We_L for the circular orifice is well above the value of 8, which is the required minimum for the formation of a jet. Also the corresponding We_G value is below 0.4 for pressures up to 10 psi (0.17 MPa). Thus, till 10 psi, the circular jet is under the Rayleigh breakup regime. The droplet formation occurs several jet diameters away from the orifice, and the drop size (average diameter

of 0.55 mm) is comparable to the equivalent jet diameter. The droplet size was measured based on the equivalent diameter of the pixel area covered by the droplets. The same can also be seen in Fig. 6. Moreover, drops are pinched off from the end of the jet. As the We_L number further increases with increase in injection pressure, the jet breaks up into ligaments in place of drops. These ligaments after travelling downwards further break up into drops under the effect of aerodynamic forces, showing the same behavior as observed by Grant and Middleman (1966). Further increase in We_L leads to the development of waves on the jet surface. These waves are clearly visible on the jet injected at 200 psi (1.48 MPa). As per the criteria mentioned earlier, the circular jet is in first wind-induced regime for pressures up to 250 psi (1.83 MPa) and is in the second wind-induced regime for pressures from 500 to 1,000 psi (3.55–6.99 MPa). This is clearly visible from the images of 500, 750, and 1,000 psi (3.55, 5.27, and 6.99 MPa). As the jet enters from first wind-induced in second wind-induced regime, the flow interaction with the ambient atmosphere changes. With an increase in jet velocity, the gas Weber number, We_G , also increases, which implies stronger aerodynamic forces act on the jet.

As a result, in second wind-induced regime, several jet diameters downstream the jet its surface starts stripping off and the breakup does not occur on the entire cross section. Moreover, the droplets formed are much smaller than the jet diameter. The trend of the breakup curve can be seen from the bars drawn on the images at the corresponding breakup locations. As expected, the breakup length increases during the first wind-induced regime, reaches its peak, and with the onset of second wind-induced regime, it starts decreasing. However, these observations are somewhat different from the breakup regimes given in the plots from a review paper (Fig. 2, Lin and Reitz 1998), which

states that the peak breakup length should occur between the transitions from the Rayleigh breakup regime to the first wind-induced breakup regime. This discrepancy is believed to be due to the nozzle geometry effects as discussed in the paper (Lin and Reitz 1998). The current circular nozzle has a length-to-diameter ratio around 4, which is short for flow to become fully developed in the nozzle. On the other hand, the results in this work show similar trend to some previous results (Hiroyasu et al. 1982; Fig. 2.15, p. 96, Lefebvre 1989). The effects of length-to-diameter ratio on the breakup regime is also clearly shown in the previous results and its can shift the breakup length peak.

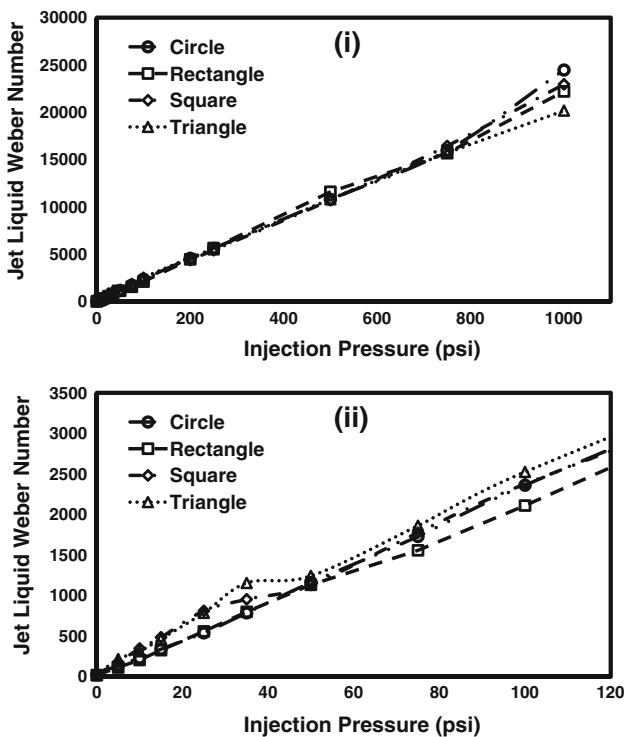
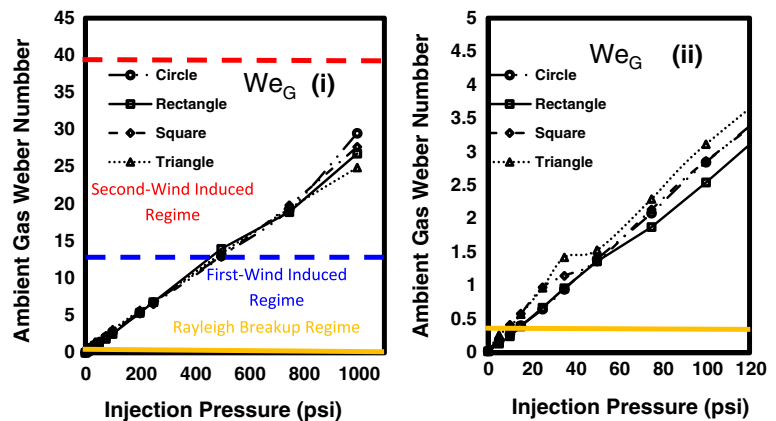


Fig. 4 The liquid Weber numbers for the four orifices under different pressures: **i** entire pressure range, and **ii** at low-pressure range (from 0 to 120 psi)

Fig. 5 The gas Weber numbers for the four orifices under different pressures: **i** for the entire pressure range, and **ii** for low injection pressures (from 0 to 120 psi)



4.2.2 Rectangular orifice

The development of the flow behavior from the rectangular orifice is depicted pictorially in Fig. 7. The images are presented in pairs. For each pair, the images were taken from two different orientations by placing the high-speed camera in two orthogonal planes, viewing the longer side (now referred to as view “RL”) and the shorter side (now referred to as view “RS”). The first image in each pair corresponds to the one taken viewing the longer side, i.e., view “RL.” The resolutions of the images for the two orientations are different for all the pressures. As a result, the scale is different for the images in each pair as indicated in Fig. 7 for different pressures. This is the reason that the jet in the second images in each pair looks smaller and thinner. For 0 psi (0.10 MPa), the jet emanated from the rectangular orifice is similar to the circular orifice and breaks up nearly axisymmetrically. The jet is completely different from the circular jet at 5 psi (0.13 MPa). Thus, for flow with liquid Weber numbers between 19.69 (corresponding to 0 psi) and 114.10 (corresponding to 5 psi), the rectangular jet behaves similar to the circular jet. This is because the surface tension forces are dominant in this regime and seek minimum surface area, thereby suppressing any effect of the asymmetric orifice. Thus, the jet

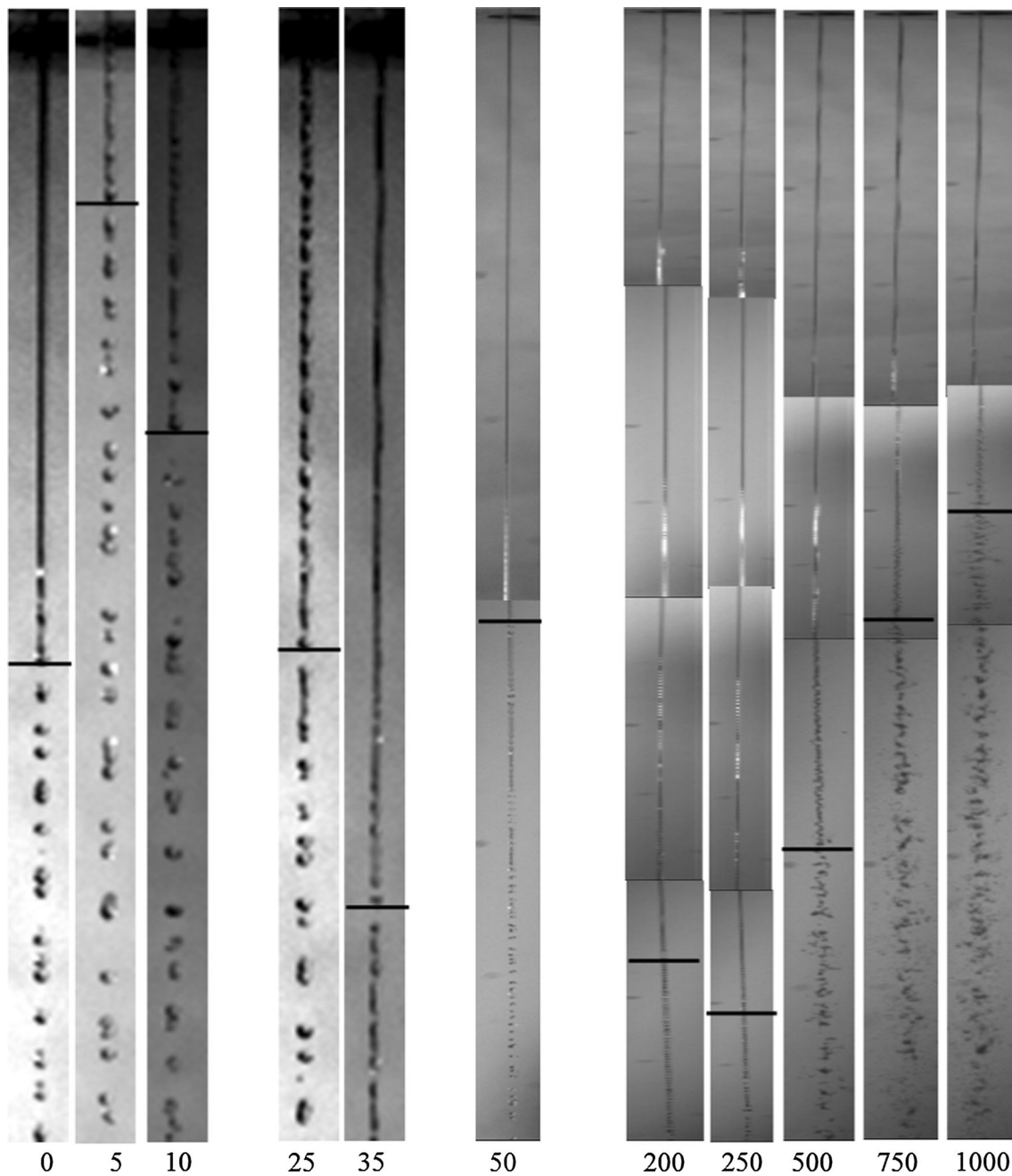


Fig. 6 Evolution of the circular jets under different flow conditions. The image sizes are 45 mm by 2.5 mm (0, 5, 10, 25, 35 psi), 160 mm by 5 mm (50 psi), and 310 mm by 5 mm (200, 250, 500, 750, 1,000 psi). Note that the width and height are not in scale for pressures > 35 psi. *Black bars* locate instantaneous breakup points.

transforms into a cylindrical jet after coming out from the rectangular orifice. This behavior is similar to that observed from the elliptical orifice by Kasyap et al. (2008, 2009). The breakup of the jet in this regime is the same as Rayleigh regime. The drops (average diameter 0.58 mm) formed are bigger than the equivalent jet diameter (0.3 mm) and are formed by pinching off from the jet's end.

Numbers below the images indicate the injection pressure in psi. Breakup regimes based on the gas Weber number are Rayleigh breakup (0, 5, 10 psi), first wind-induced breakup (25, 35, 50, 200, 250 psi), and second wind-induced breakup (500, 750, 1,000 psi)

For 5 psi (0.13 MPa), the jet acquires an entirely different shape. In view “RL,” the jet comes out of the orifice with a width corresponding to the length of the longer side of the orifice. As it moves downstream, the jet width decreases and a “neck” is formed. Further downstream, the jet width again increases and forms a crest. This behavior is repeated periodically along the jet length, and the jet periodically varies its width in the two planes. This

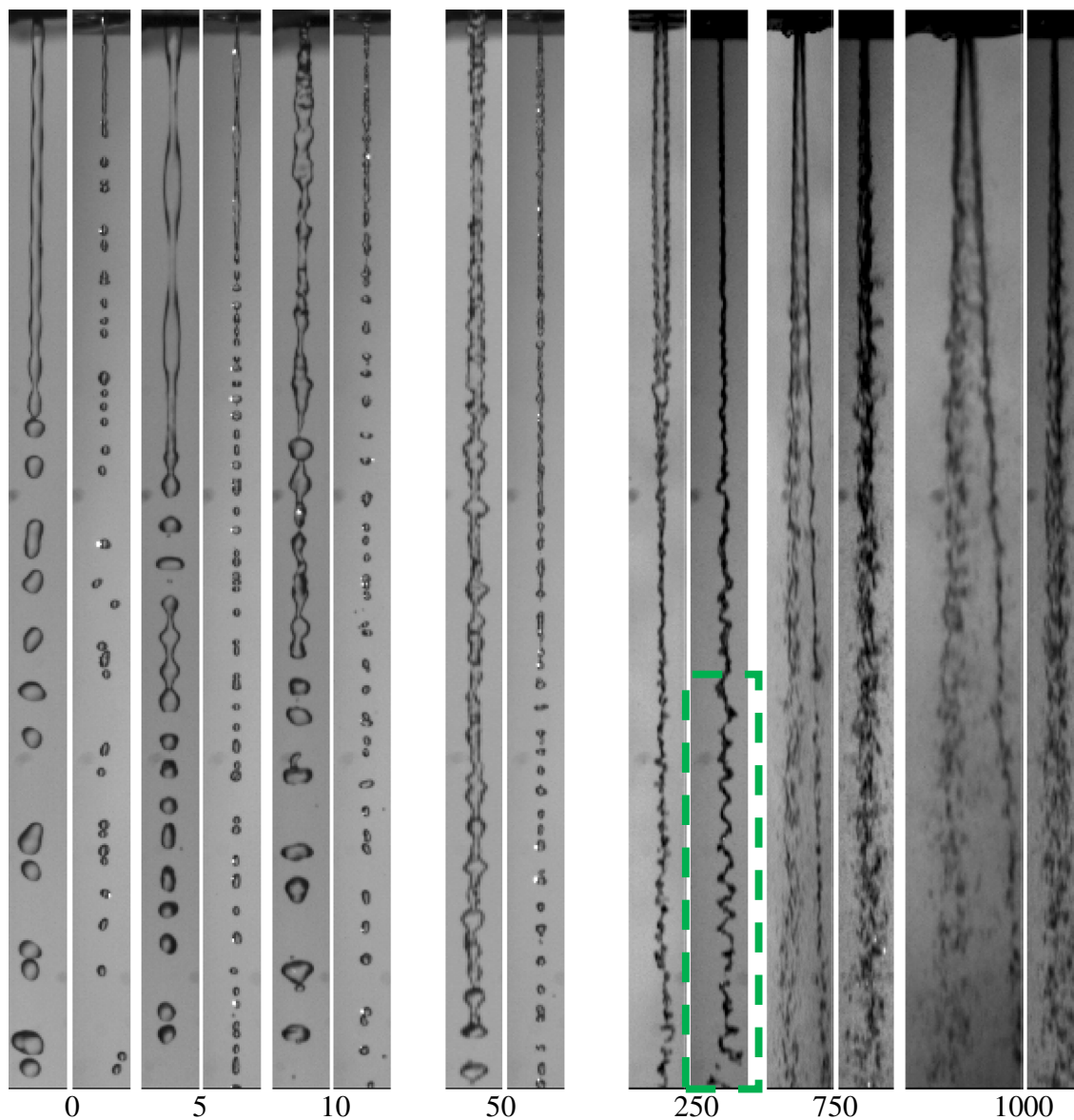


Fig. 7 Evolution of the rectangular jets under different flow conditions. First image in each pair belongs to the view “RL” while the second one to the view “RS.” Numbers indicate the injection pressure in psi. *Dashed green box* at 250 psi indicates the presence of transverse waves. The height is 85 mm for all “RS” images, and for

“RL” images, the heights are 35 mm (0, 5, 10 psi), 40 mm (50 psi), and 85 mm (250, 750, 1,000 psi). The width is in scale with the height. Breakup regimes based on the gas Weber number are Rayleigh breakup (0, 5, 10 psi), first wind-induced breakup (50 psi), and second wind-induced breakup (250, 750, 1,000 psi)

behavior is same as what has been defined as the axis-switching phenomenon. Thus, the asymmetric geometry of the orifice resulted in axis-switching phenomenon as has been observed in elliptical orifices (Kasyap et al. 2008, 2009; Ho and Gutmark 1987; Husain and Hussain 1983; Hussain and Husain 1989). The axis switching occurs multiple times because of the interaction between surface tension and inertia forces (Kasyap et al. 2008). Due to axis switching, the jet surface appears to be in the form of a spatial wave.

With increase in We_L , the surface of the jet gets ruffled. Though the axis-switching phenomenon is still visible, the jet surface has been greatly deformed by some new disturbances. These disturbances arise because of other factors including turbulence and aerodynamic forces (Kasyap et al. 2008, 2009). From the values of the Re and We_G , the jet remains laminar till 15 psi (0.20 MPa) and We_G for 10 psi (0.17 MPa) is 0.25, which is very close to 0.4. As mentioned by Miesse (1955), Pan and Suga (2006), and Reitz (1978), the effect of ambient gas becomes visible at We_G

nearly equal to 0.4. Thus, aerodynamic forces seem to be responsible for the development of surface ruffles, which start to originate from 10 psi. It can be noted that the wavelength of the axis-switching phenomenon increases with increase in injection pressure or jet Weber number. It has been observed by Rayleigh (1879) and Geer and Strikwerda (1983) that the wavelength varies linearly with the Weber number. In the image for 200 psi (1.48 MPa), one crest can be seen in view “RL” just after which the jet gets disrupted. For pressures above 250 psi (1.83 MPa), it can be seen that the crest is formed right after the orifice exit but the wavelength of the crest is greater than the breakup length of the jet and hence, the jet disrupts before the jet converges to form a neck. Furthermore, the development of some transverse waves can be seen in the images of view “RS” at 200 psi. Depending on the wavelength of the axis-switching process and the location of the transverse waves, the jet width should be higher in “RL” view. Thus, the jet behaves like a thin sheet whose plane is perpendicular to the “RS” view plane. Thus, the liquid sheet develops transverse waves similar to those developed on planar liquid sheets (Kasyap et al. 2009). These waves are present only in “RS” plane and seem to originate at 200 psi, and by 250 psi, they become so violent to cause the jet to break up. For high injection pressures, such as 1,000 psi (6.99 MPa), the jet opens and forms a fan shape spray with wide angle in the long side and small angle in the short side. Small droplets are torn off from the edge of the jet.

With regard to the droplet formation, it can be noted from the images that up to 10 psi, the droplets formed are nearly twice in size as the hydraulic diameter (drop diameter around 0.58 mm). For higher pressures, the jet breakup results in the formation of ligaments. Possibly, the necks formed due to axis switching tend to act like weak points that are susceptible to the growing disturbances and the portion of the jet beyond the neck breaks off as a ligament. Moreover, the jet produced from rectangular orifice is more of a liquid sheet than a jet. Hence, the droplets formed are expected to be in the form of ligaments that may further breakup into drops.

4.2.3 Square orifice

The development of the jets from the square orifice is presented for varying injection pressures in Fig. 8. Images are provided in groups of three. Each group corresponds to different pressure. However, the images have been taken from three different planes of view. The first two images were taken viewing two different sides of the square orifice at right angles and from now on will be referred to as view “SF” and view “SS,” respectively. The third images were taken from the plane of view in line with one of the diagonals of the square orifice, thus looking at one of its

vertices. This will be referred to as view, “SV.” Once again, significant differences can be observed both from the circular jet as well as the rectangular jet. However, since the square orifice and so does the triangular orifice lack aspect ratio effects in their geometry, their jets are expected to be somewhat similar to the circular orifice. Whatever changes that are presented can, thus, be attributed to the presence of sharp corners in square and triangular geometry. Being non-circular geometries, both square and triangular jets are also expected to demonstrate the axis-switching phenomenon. Since the differences in the widths in the different view planes are zero or very small, therefore, it is very difficult to determine the presence of axis switching visually.

At 0 psi (0.10 MPa), the jet is under the effect of strong surface tension forces and appears to come out as a thin cylindrical jet, i.e., the effect of the presence of asymmetric geometry has been suppressed. Thus, the jet is similar to a cylindrical jet and undergoes breakup through Rayleigh mechanism. With increase in the Weber number, the smooth jet surface is lost and various perturbations arise on the jet surface. Based on the Reynolds numbers, the jet from the square orifice is the first to become fully turbulent at 25 psi (0.27 MPa) while circular and triangular jets show turbulence at 35 psi (0.34 MPa). But even for pressures below 25 psi, i.e., 10 and 15 psi (0.17 and 0.20 MPa), the surface of the square jet appears more ruffled. The jet enters first wind-induced regime ($We_G > 0.4$) at 10 psi only while the circular jet has entered it at 15 psi. Thus, it is expected that some factors are present, which are inducing turbulence at a quicker rate and augmenting the effect of ambient gas at a higher rate in the square jets as compared to the circular jets. These factors might include the differences in the exit velocity and the hydraulic diameter, and the corners of the square orifice.

Regarding the breakup of the square jet, it can be seen that with increase in We_L , the breakup length of the jets is increasing. Moreover, the droplets are pinching off from the jet and are of nearly the same size as the jet equivalent diameter. This can be seen in Fig. 8. Thus, the jet behavior corresponds to the first wind-induced regime. At higher injection pressures, square jets also tend to breakup in the form of ligaments. Transverse waves (highlighted in a box) can also be observed far away from the orifice for injection pressures of 500 psi (3.55 MPa) and above. In rectangular jets, these waves have appeared at a comparatively lower pressure of 200 psi (1.48 MPa) (Fig. 7). The presence of such transverse waves indicates the sheet-like behavior of the square jet similar to rectangular jets. Based on the We_G value in Figs. 4 and 5, it can be seen that the square jets enter the second wind-induced regime at 500 psi (3.55 MPa) ($We_G \approx 13$) just like jets from other orifices. As per the second wind-induced regime, the jets for

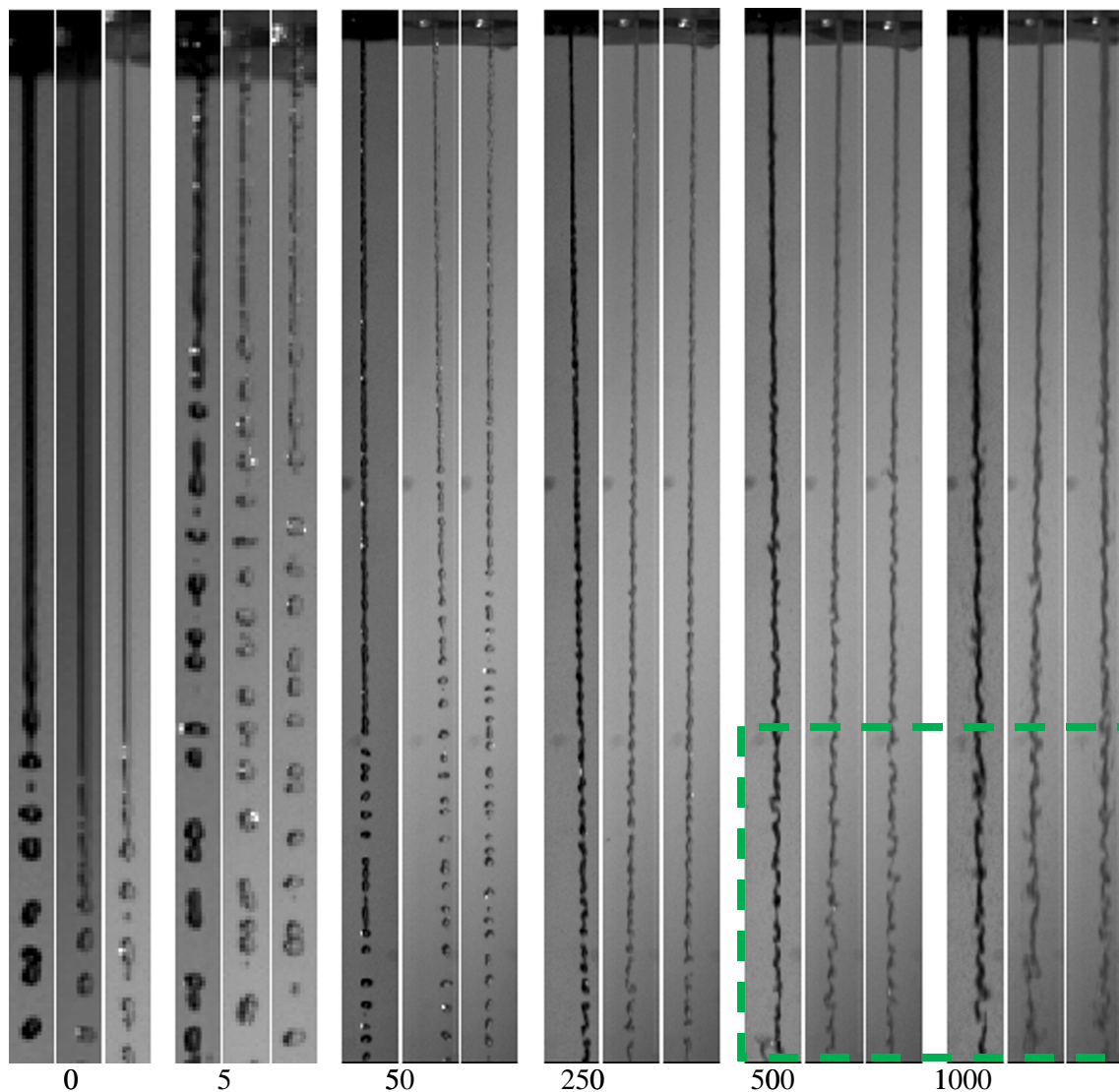


Fig. 8 Evolution of the square jets under different flow conditions. Images are in groups of 3. The first image belongs to the “SF” view, the second image belongs to the “SS” view, and the last image belongs to the “SV” view. *Numbers* indicate the injection pressures in psi. *Dashed box* shows the presence of transverse waves at injection

500 psi, and higher injection pressures, the jet surface has begun to strip off but still this process is not prominently visible at 500 psi. The droplets generated from surface disruption are visually much smaller than the jet equivalent diameter. Additionally, a considerable increase in jet width can be observed for injection pressures from 250 to 1,000 psi (from 1.82 to 6.99 MPa). This is because of the turbulence and increasing effect of the aerodynamic forces.

4.2.4 Triangular orifice

In the case of the triangular orifice, the images were taken from two different planes of view. One looking at one of

pressures of 500 and 1,000 psi. The height is 30 mm for 0 and 5 psi, and is 60 mm for the rest injection pressure. The width is in scale with the height. Breakup regimes based on the gas Weber number are Rayleigh breakup (0, 5 psi), first wind-induced breakup (50, 250 psi), and second wind-induced breakup (500, 1,000 psi)

the sides of the triangular orifice, which will be referred to as view “TS” and the other looking at one of the vertices, which will be called, view “TV.” Thus, for each injection pressure, a pair of images is shown in Fig. 9. The behavior of the triangular jet at 0 psi (0.10 MPa) is similar to the circular jet. Owing to the strong surface tension forces at this We_L , the effects of the triangular geometry have been suppressed. The jet breaks up as per the Rayleigh regime (drop diameter around 0.74 mm). As the We_L increases, the effects of the presence of sharp corners become evident. Surface perturbations arise with increase in injection pressure. As seen in Fig. 3 even at low injection pressure of 10 psi (0.17 MPa), the jet is no more laminar and is

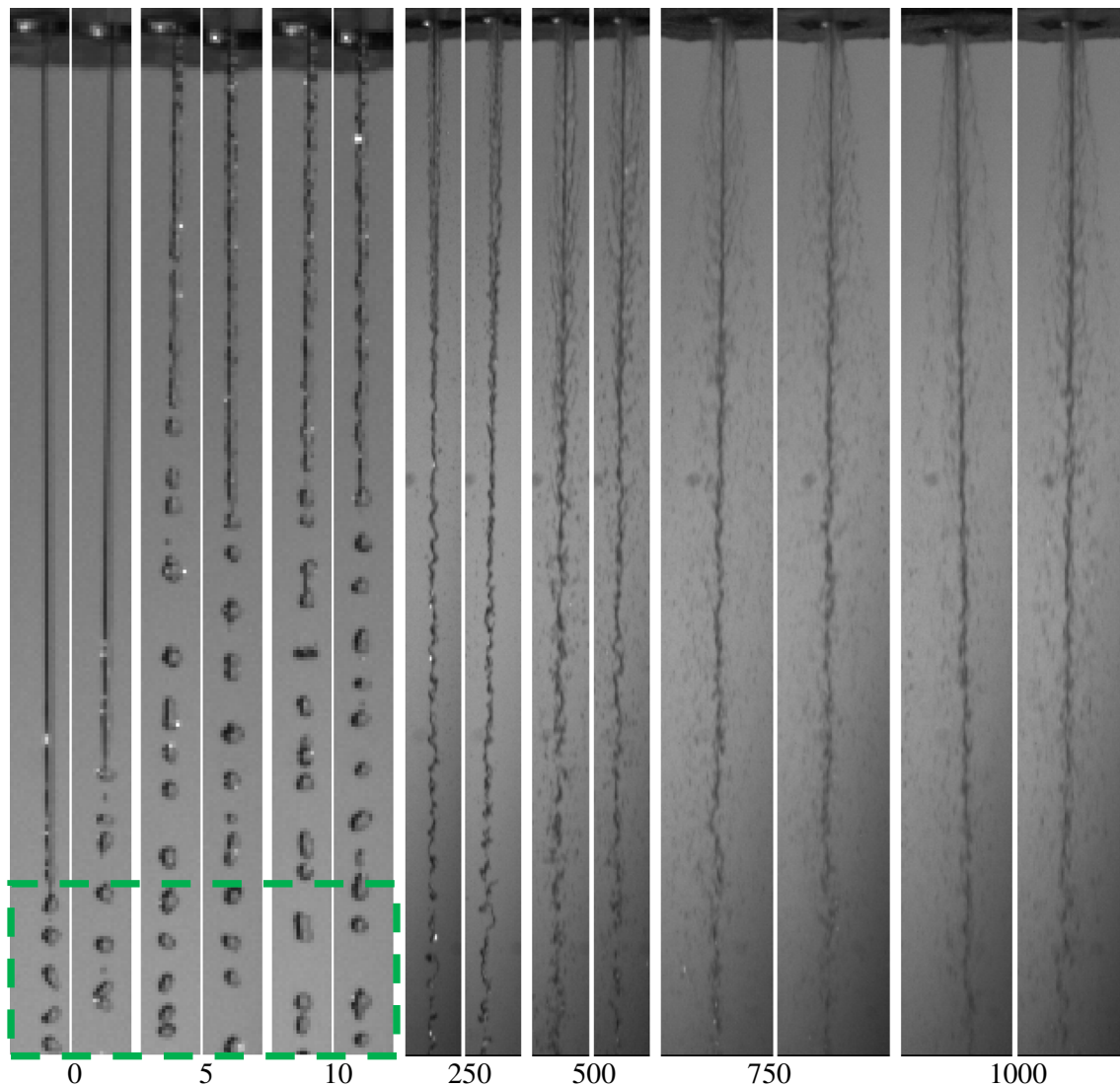


Fig. 9 Evolution of the triangular jets under different flow conditions. Images are in pairs. The first image belongs to the “TS” view and the second image belongs to the “TV” view. Numbers indicate the injection pressures in psi. The image height is 45 mm for 0, 5, and 10 psi, and is 90 mm for the rest injection pressures. The width is in

scale with the height. Breakup regimes based on the gas Weber number are Rayleigh breakup (0, 5 psi), first wind-induced breakup (10, 250 psi), and second wind-induced breakup (500, 750, 1,000 psi). The box highlights that the droplet size is comparable to the jet equivalent diameter in Rayleigh and first wind-induced regime

undergoing transition to turbulence. Also, the We_G value has reached the limiting value of 0.4 and, thus, has entered the first wind-induced regime (Figs. 4, 5). This indicates that there is a strong interaction of the jet with the ambient gas. The jet has not attained turbulence and does not demonstrate the phenomenon of axis switching. As mentioned in the previous section, square jets were showing a similar behavior. Since the We_G value is higher for triangular jet, this strong atmospheric interaction can be attributed to the higher jet velocity. As expected and mentioned earlier, due to the presence of sharp angles in the orifice geometry, the interaction of the triangular jet is similar to the square jet. The droplets formed in the first

wind-induced regime visually seem comparable with the jet equivalent diameter (drop diameter around 0.78 mm). The same is highlighted in Fig. 9. With the increase in We_L , ligaments break off from the jet, which undergo further breakup. The jet surface is very close to disruption at 250 psi (1.82 MPa). At injection pressures of 500 psi (3.55 MPa) and above, the jet is in the second wind-induced regime and its surface can be seen to strip off and the resultant droplets produced are very small as compared to the jet diameter. In fact, at injection pressures of 1,000 psi (6.99 MPa) (Fig. 9), the jet shows many fine structure near the nozzle with a very wide angle in both “TS” and “TV” views, which is similar to the long side of

the rectangular orifice. This structure is very different from circular and square nozzles, which can provide potential benefits for liquid atomization. Similar to the square jets, no appreciable axis-switching phenomenon is visible in triangular jets.

The breakup behavior of the asymmetric jets described in this section has been based on the different regimes mentioned in Figs. 4 and 5. The definitions of different regimes shown in Figs. 4 and 5 were defined for circular jets, and it is expected that the ranges of these regimes may not be readily applicable to asymmetric jets. However, the classifications of different regimes seem applicable to asymmetric jets, too. Moreover, the ranges were defined based on the interaction of ambient gas inertial and surface tension forces. Even though the asymmetric jets have enhanced disturbances due to the non-circular geometry, those disturbances are not included in defining the ranges for different regimes. It should be noted that these parameters may have limitations to show the complete behavior of the jet breakup and cannot account for the new features from non-circular jets. The values of the critical gas Weber number for different breakup regimes are also expected to be different from circular nozzles. More systematic investigations are necessary to provide more insights into the non-circular liquid jets.

4.3 Comparison of the breakup behavior

The cine files recorded using the high-speed camera have been processed using the Image Processing Toolbox of MATLAB. Each frame of the cine files has been converted into an image. These images were then subjected to edge detection using an edge detection algorithm after required cropping and contrast adjustment. The binary images, thus, obtained were used for the measurement of the jet breakup length. The image was analyzed along its length, and the first location of jet detachment was marked and noted as the jet breakup length.

For each injection pressure, five shots of the steady-state liquid jets were taken. Each shot comprised of 1,000 frames. Thus, for each flow condition, 5,000 different images of jet breakup phenomenon have been evaluated. Figure 10 depicting the variation of the breakup length for different jets at varying flow conditions has been prepared using the average value of the 5,000 images for each injection pressure. As mentioned, the values in the chart represent the average values and should not be compared with the instantaneous lengths depicted in the images of the jets provided in the previous section. Jet breakup is a dynamic phenomenon. Even for given flow conditions, it is a result of continuous interaction between a number of forces including the inertia, surface tension, viscosity and aerodynamic, turbulence, and cavitation effects. As a

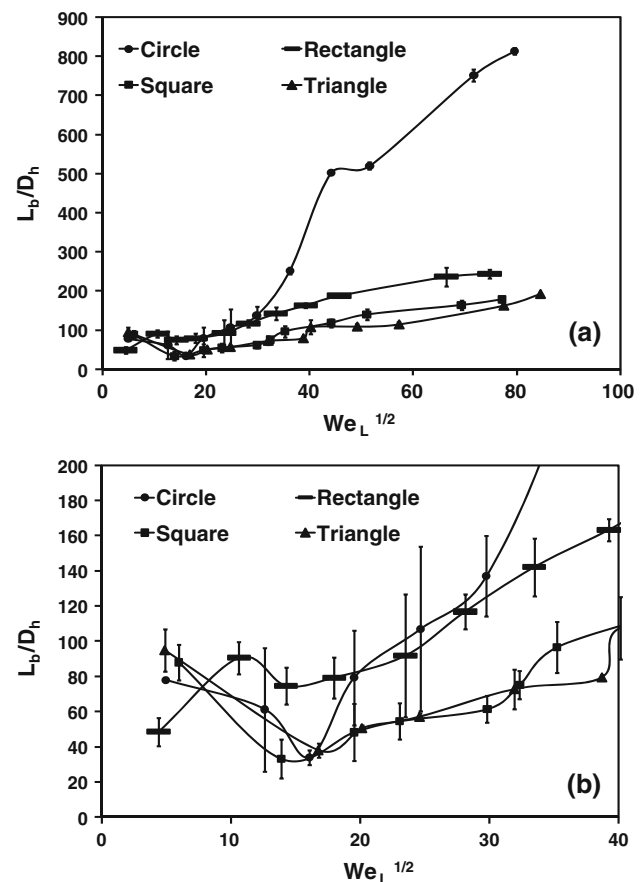


Fig. 10 The non-dimensionalized breakup length at low $\sqrt{We_L}$ conditions **a** entire range; **b** magnified view for the low range

result, the jet breakup length varies continually with time along the jet axis. However, this temporal variation is different from the one induced due to change in flow conditions. Thus, once again, the time-averaged breakup length should not be confused with the instantaneous breakup lengths. Owing to the differences in the geometries, the measurements of the breakup length, L_b , have been non-dimensionalized or normalized by dividing them with the corresponding hydraulic diameters of their orifices. The normalized breakup lengths have been plotted against the $\sqrt{We_L}$ values. Weber number is a non-dimensional parameter, which describes the qualitative aspects of jet breakup and also gives linear dependence of the breakup length with the jet injection velocity (Fig. 10). It also emphasizes on the significant role played by surface tension in jet breakup. Axis-switching phenomenon is an outcome of interaction between inertial and surface tension forces and greatly impacts the breakup length of jets from non-circular orifices. Thus, using Weber number for characterizing the breakup phenomenon seems an appropriate choice. Although the We_L value is different for the different orifices at different injection

pressures, still the values are in close range with each other.

The chart has been plotted for injection pressures up to 250 psi (1.82 MPa). For the remaining higher injection pressure, it was difficult to accurately measure the breakup length. This is because all the jets enter the second wind-induced regime at injection pressures above 250 psi (1.82 MPa), which makes the clear identification of breakup location difficult. The chart clearly demonstrates the difference in the breakup length obtained from circular and non-circular orifices. The breakup lengths for all the orifices have increases nearly linearly as expected from the Rayleigh and first wind-induced regimes. Interestingly, the normalized breakup lengths from the non-circular orifices tend to coincide with each other, and the maximum value obtained at 250 psi (1.82 MPa) is only 30 % of the normalized breakup length from circular orifice under identical flow conditions. This emphasizes on the fact mentioned in Sect. 4.2 that asymmetric geometry and phenomena like axis switching and transverse waves induce enhanced unstable growths to the liquid jet as compared to the circular orifice. Thus, the instabilities experienced by non-circular jets are different from those experienced by circular jets. The same behavior was observed by Kasyap et al. (2008, 2009) and Amini and Dolatabadi (2012) in elliptical orifices. Thus, the breakup lengths of the jets obtained from circular orifice at different flow conditions are greater than those of the jets obtained from non-circular orifices.

However, for flow conditions corresponding to 35 psi (0.34 MPa), the normalized breakup lengths obtained from all the orifices appear to be close. This has been highlighted on the chart. A closer look at the chart under these conditions reveals that except the rectangular orifice, breakup lengths from all other orifices tend to follow the same trend. Similar behavior was observed from the visual inspection of the images where at low We_L conditions, the square and triangular jets tend to behave like a circular jet owing to the dominant surface tension forces. It can be seen that the breakup lengths of the jets from circular, square, and triangular orifices are decreasing from an initial value, reach a minimum, and then increase again. But the rectangular jets have followed a different trend. The breakup lengths of rectangular jets have shown a positive slope with injection pressures. Since the jets from rectangular orifices have demonstrated axis switching starting from pressures like 5 psi (0.13 MPa), the difference in the behavior of rectangular jets from other jets can be attributed to the axis-switching phenomenon. After a certain threshold, We_L is achieved for injection pressures above 35 psi (absolute 0.34 MPa), even square and triangular jets tend to deviate from the circular jet behavior and the breakup lengths obtained from rectangular, square, and triangular jets are nearly the same. This similarity points

out that under these flow conditions, all the non-circular jets are experiencing a common phenomenon. Rectangular, square, and triangular orifices all are asymmetric and have sharp corners, but the latter two lack the aspect ratio effects present in the rectangular shape. The axis-switching phenomenon is prominently visible in rectangular orifices due to the aspect ratio effect in the geometry. Since the square and triangular orifice lack this feature, it is quite possible that axis switching is present but not clearly visible. In the following section, it has been explained on the basis of jet width measurement that the square and triangular jets lack axis-switching phenomenon for injection pressures below 35 psi (0.34 MPa). This further supports the similarity between circular jets and square and triangular jets and their differences from the rectangular jets at injection pressures below 35 psi.

4.4 Jet width measurement

Due to axis switching for a rectangular jet, if the width is greater in major axis plane, it will gradually reduce and the width in the minor axis plane will gradually increase. Eventually, the jet width in the major axis plane will become smaller than the jet width in the minor axis plane. During the complete change in the orientation, the jet widths in two planes will nearly be the same at one point and this is when the jet acquires a circular cross section. Based on this assumption, the jet width for all the flow conditions was measured. For each flow condition, an average of jet width from 5,000 different images has been calculated. The width measurement has been carried out only till the breakup location of the jets.

For rectangular orifice, the axis switching is not visible at 0 psi (0.10 MPa) and the jet is said to be behaving like a circular jet. But the widths in the two view planes are completely different and increase linearly along the jet axis. Though the jet appeared cylindrical, actually the behavior is different. The behavior of the jet widths in the two orientations at pressures above 0 psi is the same as what was expected and is shown for 15 (0.20 MPa) and 250 psi (1.82 MPa) in Fig. 11. Hence, it can be seen that

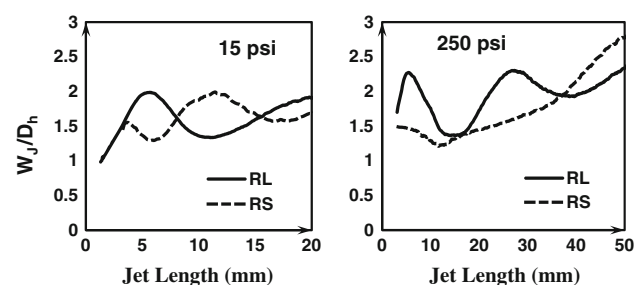


Fig. 11 Variation of normalized jet width from rectangular orifice in different view planes at 15 and 250 psi

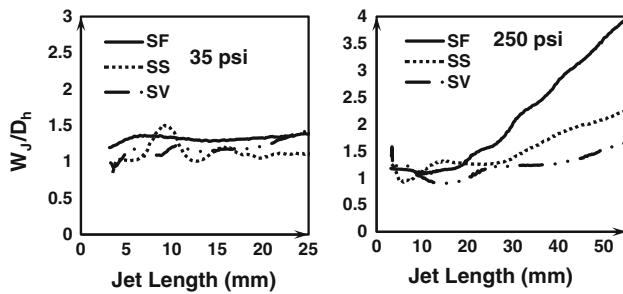


Fig. 12 Variation of normalized jet width from square orifice in different view planes at 35 and 250 psi

plotting the jet width along the jet axis can easily depict the phenomenon of axis switching.

For square orifices, for pressures up to 35 psi (0.34 MPa), the jet widths in the three view planes remain nearly constant along the jet axis with slight variations as can be seen in Fig. 12. Thus, the jet remains nearly symmetric and behaves similar to the circular jet up for flow conditions up to 35 psi. Beyond 35 psi, variation in jet widths starts to appear along the jet axis. The variations increase with injection pressures. At 250 psi (1.82 MPa), it can be seen that for jet length up to 20 mm, the jet width is nearly same in all three view planes. This represents the circular cross section. However, beyond 20-mm jet length, the widths start to deviate from each other. As we go further downstream, it can be seen that the width is the maximum in “SF” view plane, followed by the jet width in “SS” view plane and it is the minimum in “SV” view plane. The variation in jet width in different view planes corresponds to axis switching. Thus, it can be concluded that axis switching is not present for flow conditions corresponding to injection pressures of 35 psi and below and can only be seen at injection pressures above 35 psi.

Similar to the square orifice, the triangular jet width in the two different planes of view for the triangular orifice starts to differ from 50 psi (0.44 MPa) as can be seen in Fig. 13. At 250 psi (1.82 MPa), it can be seen that the jet widths in the two planes are same at the orifice exit. Further, “TV” width is greater than “TS” width. As the jet moves downwards, both the jets become equal. Further downstream, the “TS” width becomes greater than the “TV.” Since the triangular orifice does not have any kind of symmetry in its geometry, the behavior observed is slightly different from the square orifice. Thus, for injection pressures of 35 psi (0.34 MPa) and below, the axis-switching phenomenon is not obvious in the square and the triangular orifice and the jets behave like a cylindrical jet. As a result, even the breakup lengths of the jet are same as the circular jets under similar flow conditions. As axis-switching phenomenon becomes visible at injection pressures of 50 psi (0.44 MPa) and above, the behavior of the

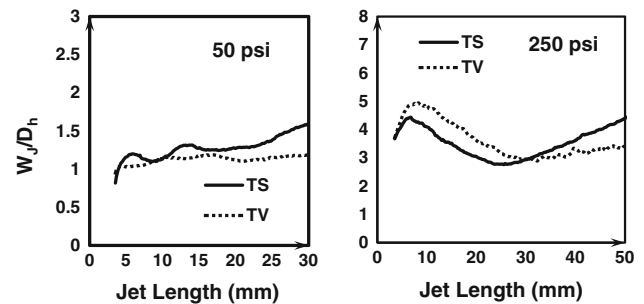


Fig. 13 Variation of normalized jet width from triangular orifice in different view planes at 50 and 250 psi

square and triangular jets begin to differ from the circular jets. As a result, a deviation in the jet breakup length behavior can be observed at these flow conditions. Thus, it can be concluded that non-circular geometry results in the axis-switching phenomenon, which introduces enhanced instability in the jets, thereby leading to shorter breakup lengths and faster and more severe jet disintegration.

5 Conclusions

The effects of the non-circular orifices on the breakup phenomena of water jets are evaluated experimentally. The flow behavior was characterized using the non-dimensional parameters like the Reynolds number and the Weber number. The breakup phenomenon was characterized by measuring the breakup lengths and jet width of the low-pressure jets obtained from the non-circular orifices. Depending on the gas Weber number, different breakup regimes were identified and it was observed that under the experimental flow conditions, the jets experienced the Rayleigh, the first wind-induced, and the second wind-induced breakup regimes under the experimental flow conditions. The non-circular jets demonstrated enhanced unstable behavior and exhibited faster breakup process as compared to the corresponding circular jets. The breakup lengths for the non-circular jets tended to coincide with each other and were markedly smaller than the breakup length of the circular jets. Moreover, the rectangular jets prominently displayed the axis-switching phenomenon. The square and triangular jets behaved like the circular jets for a specific range of flow conditions and did not display the axis-switching process. For the flow conditions away from this range, the square and triangular jets behavior deviated from the circular jet behavior and exhibited faster breakup process. However, the axis-switching phenomenon was not obvious from the images under any flow conditions for the square and triangular jets. For higher injection pressures, variations in the quantitative jet widths were obtained in the different view planes, which proved the existence of the axis-switching

phenomenon in the square and triangular jets. The phenomenon was prominently visible in the rectangular jets due to its aspect ratio effect of geometry. The faster jet breakup observed in non-circular jets can, thus, be attributed to the axis-switching phenomenon as well as orifice geometry. Moreover, it can be inferred that the non-circular orifice geometry induces greater instabilities in the jet and causes it to disintegrate faster.

Acknowledgments The authors express their sincere gratitude to the reviewers for their time, interest, and constructive suggestions for the significant improvement of the paper. This research was supported in part by the Research and Innovation Seed Funding (RISF) program at the North Carolina State University.

References

- Amini G, Dolatabadi A (2012) Axis-switching and breakup of low-speed elliptic liquid jets. *Int J Multiph Flow* 42:96–103
- Bidone G (1829) Experiences sur la forme et sur la direction des veines et des courants d'eau lances par diverses ouvertures. Imprimerie Royale, Turin, pp 1–136
- Drazin PG, Reid WH (1981) Hydrodynamic stability. Cambridge University Press, Cambridge
- Geer JF, Strikwerda JC (1983) Vertical slender jets with surface tension. *J Fluid Mech* 135:155–169
- Grant RP, Middleman S (1966) Newtonian jet stability. *AICHE J* 12:669–678
- Gutmark EJ, Grinstein FF (1999) Flow control with noncircular jets. *Annu Rev Fluid Mech* 31:239–272
- Herzberg J, Ho CM (1995) Three dimensional vortex dynamics in a rectangular sudden expansion. *J Fluid Mech* 289:1–27
- Hiroyasu H, Shimizu M, Arai M (1982) The breakup of high speed jet in a high pressure gaseous atmosphere. In: Proceedings of the 2nd international conference on liquid atomization and spray systems, Madison, WI, pp. 69–74
- Ho CM, Gutmark EJ (1987) Vortex induction and mass entrainment in a small-aspect ratio elliptic jet. *J Fluid Mech* 179:383–405
- Husain HS, Hussain AKMF (1983) Controlled excitation of elliptic jets. *Phys Fluids* 26:2763–2766
- Husain AKMF, Husain HS (1989) Elliptic jets part I. Characteristics of unexcited and excited jets. *J Fluid Mech* 208:257–320
- Kasyap TV, Sivakumar D, Raghunandan BN (2008) Breakup of liquid jets emanating from elliptical orifices at low flow conditions. *At Spray* 18:645–668
- Kasyap TV, Sivakumar D, Raghunandan BN (2009) Flow and breakup characteristics of elliptical liquid jets. *Int J Multiph Flow* 35:8–19
- Konkachbaev AI, Morley NB, Gulec K, Sketchley T (2000) Stability and contraction of a rectangular liquid metal jet in a vacuum environment. *Fusion Eng Des* 51–52:1109–1114
- Lefebvre AH (1985) Fuel effects on gas turbine combustion—ignition, stability, and combustion efficiency. *ASME J Eng Gas Turbines Power* 107:24–37
- Lefebvre AH (1989) Atomization and sprays. Hemisphere, New York
- Lin SP (1996) Regimes of jet breakup and breakup mechanisms. In: Kuo KK (ed) Recent advances in spray combustion: spray atomization and drop burning phenomena, vol I. AIAA Inc, Virginia, pp 137–160
- Lin SP (2003) Breakup of liquid sheets and jets. Cambridge University Press, New York
- Lin SP, Reitz RD (1998) Drop and spray formation from a liquid jet. *Ann Rev Fluid Mech* 30:85–105
- Messina T, Acharya S (2006) Characteristics of an acoustically modulated spray issued from circular and elliptical orifice nozzles. *At Sprays* 16:331–348
- Miesse CC (1955) Correlation of experimental data on the disintegration of liquid jets. *Ind Eng Chem* 47:1690–1695
- Munson BR, Okiishi TH, Huebsch WW, Rothmayer AP (2013) Fundamentals of fluid mechanics, 7th edn. Wiley, London, p 403
- Ohnesorge W (1936) Formation of drops by nozzles and the breakup of liquid jets. *Z Angew Math Mech* 16:355–358
- Pan Y, Suga K (2006) A numerical study on the breakup process of laminar liquid jets into a gas. *Phys Fluids* 18:052101
- Plateau J (1873) Statique experimentale et theorique des liquides soumis aux seules forces moleculaires (Cited by Lord Rayleigh, *Theory of Sound*, Vol. II, p. 363, 1945. New York: Dover)
- Ranz WE (1956) On sprays and spraying: a survey of spray technology for research and development engineers, Part 1. Pennsylvania State University, Department Of Engineering Research, Bulletin No. 65
- Rayleigh L (1878) On the instability of jets. *Proc Lond Math Soc* 10:4–13
- Rayleigh L (1879) On the capillary phenomena of liquid jets. *Proc R Soc Lond* 29:71–97
- Rayleigh L (1945) The theory of sound, vol 2. Dover, New York
- Reeves CM and Lefebvre AH (1986) Fuel effects on aircraft combustor emissions. *ASME* 86-GT-212
- Reitz RD (1978) Atomization and other breakup regimes of a liquid jet. Ph.D. Thesis, Princeton University, NJ
- Reitz RD, Bracco FV (1982) Mechanism of atomization of a liquid jet. *Phys Fluids* 25:1730–1742
- Reitz RD, Bracco FV (1986) Mechanisms of breakup of round liquid jets. In: Chermisnoff N (ed) The Encyclopedia of Fluid Mechanics, vol 3. Gulf, Houston, pp 233–249
- Rink KK, Lefebvre AH (1986) Influence of fuel drop size and combustor operating conditions on pollutant emissions. *SAE technical paper* 861541
- Savart F (1833) Memoire sur la constitution des veines liquides lancees par des orifices circulaires en mince paroi. *Ann Chim Phys* 53:337–386
- Soderberg LD, Alfredson PH (1998) Experimental and theoretical stability investigation of plane liquid jets. *Eur J Mech B Fluids* 17:689–737
- Sterling AM, Sleicher CA (1975) The instability of capillary jets. *J Fluid Mech* 68:477–495
- Tyler E (1933) Instability of liquid jets. *Phil Mag* 16:504–518
- Weber CZ (1931) Zum Zerfall eines Flussigkeitsstrahles. *Math Mech* 11:136–154
- Woodyard D (2004) Pounder's marine diesel engines and gas turbines. Elsevier Ltd, Burlington, MA
- Yunyi G, Changwen L, Yezhou H, Zhijun P (1998) An experimental study on droplet size characteristics and air entrainment of elliptic sprays. *SAE paper* 982546
- Zelenka P, Krieglner W, Herzog PI, and Cartellieri WP (1990) Ways toward the clean heavy-duty diesel. *SAE paper* 900602